EXAFS study of local structure shape memory alloy $Ti_{0.5}Ni_{0.25}Cu_{0.25}$

Denis Leshchev, National Russian Nuclear University, Moscow

September 7, 2011

Abstract

Crystal structure temperature dependence of shape memory alloy (SMA) $Ti_{0.5}Ni_{0.25}Cu_{0.25}$ was investigated by means of EXAFS-spectroscopy method on beamline A1 at DORIS III on Ti K-edge. Shape memory property gives a unique ability to this type of alloys to fully restore their pre-deformed shape after being heated as a result of direct and reverse martensitic transformations. Phase transition from martensitic to austenitic phase of $Ti_{0.5}Ni_{0.25}Cu_{0.25}$ appears in temperature range of 30-70 ^{o}C, and also, that is usual for SMA, it demonstrates hysteretic properties. So for this aim was designed new sample holder, which contains Peltier modules for heating and cooling the sample and providing temperature range of 20-100 ^{o}C.

Contents

1 Introduction

1.1 $Ti_{0.5}Ni_{0.25}Cu_{0.25}$ Structure

Previously absorption spectra for Ni and Cu K-edges in $Ti_{0.5}Ni_{0.25}Cu_{0.25}$ alloy were measured at Kurchatov Institute synchrotron in Moscow, Russia. Phase transition in this sample was investigated by means of EXAFS spectroscopy from these spectra [1]. However to get complete view on process of this transition and hysteresis properties it is necessary to study absorption spectra for Ti K-edge. This edge has energy 4966 eV, and x-rays with this energy are absorbing in air, so main requirement for this experiment is high vacuum. That's why these spectra were measured on A1 beamline at DORIS III.

From X-ray structure analysis is known that alloy $Ti_{0.5}Ni_{0.25}Cu_{0.25}$ has orthorhombic B19 structure in martensitic and cubic B2 structure in austenitic phase. Ni and Cu are located in similar positions in unit cell. In austenitic phase Ti has 8 Ni/Cu atoms in first coordination shell and 6 Ti atoms in second coordination shell. In martensitic phase these spheres are additionally divided. Transition between two phases B2 and B19 occurs in following way: while being cooled B2 structure has shifts in crystallographic directions $[001]_{B2}$, $[110]_{B2}$ and $[1\underline{1}0]_{B2}$, and also there is so called δ-shift $(110)[1\underline{1}0]_{B2}$ (Fig. 1.1). For reverse transition shifts appears with B19 structure in opposite directions

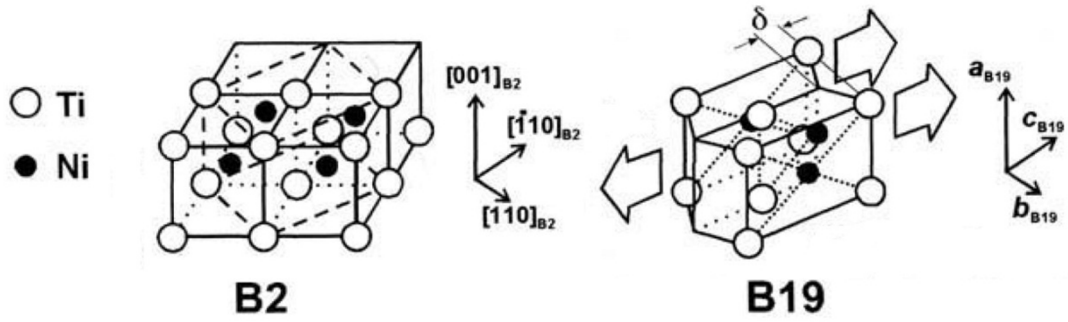

[2].

Figure 1.1 Phase transition between B2 and B19 structures.

There are lattice parameters and atomic positions in table 1. They were used for simulation of model spectra to obtain data from experimental EXAFS spectra by fitting procedure.

Table 1. Lattice Parameters and atomic positions.

Structure	Ti			Ni/Cu			a, Å	b, Å	c, Å
	x	y	z	x	y	z			
B2	0.0	0.0	0.0	0.5	0.5	0.5	3.06	3.06	3.06
B19	0.5	0.25	0.225	0.0	0.250	0.699	2.919	4.288	4.500

1.2 Shape memory properties

Shape memory ability appears due to martensitic transition - kind of polymorphic phase transition. While this transition is going, atoms are changing their positions corresponding to lattice

type of initial and final states. This movement of atoms can be produced in two ways. First, diffusional way appears when temperature of transition is high, and atoms break their atomic bonds and move to another positions individually, changing their neighbors. It's obvious, that in this case shape memory effect can't appear, because atoms don't "remember" their neighbors and deformation of alloy does not appear. Another way is when transition temperature is low. In this case diffusion doesn't cause big effect and atoms form some kind of clusters and slightly move collectively, so they don't change their neighbors. Such collective shift generates change of geometry form in areas that felt martensitic transition. Experimentally it can be observed when relief appears on pre-polished surface. Changing geometry can produce some stresses inside of alloy, and these stresses can help further transition. Thus martensitic transition is phase transition and deformation process. Saving neighbors relates this sort of deformation with elastic deformation and also its basement of shape memory property.

However, return to original form, i.e. shape memory, not always observed. There are two reasons for preventing fully structure reversibility. First reason is that for atoms it is not necessarily to move in reverse direction in back transition, because usually there is not only one direction for collective shift that changes one lattice to another. For example, for transition between cubic and rhombohedral lattices can appear in 4 directions for transition from cubic to rhombohedral lattice type and only in one direction for back transition. Number of directions for transition depends on symmetry of lattice: lower symmetry of lattice than less number of these directions. Usually symmetry of martensitic phase is lower than austenitic. Another point is an accommodation problem. While transition is going on the bound of phases stresses appear, because of difference of lattice's parameters. This difference reaches value 10-20%, so as result surrounding areas of growing phase are strongly deformed. Sometimes these deformations realize through thermo elastic martensitic transitions, so all of these deformations are reversible and this problem does not appear. That's why alloys with thermo elastic martensitic transition are identified with shape memory alloys.

2 Theory

2.1 X-ray absorption spectroscopy. EXAFS.

X-rays are electromagnetic waves which have wavelengths in the range of ~0.1-100 Å and corresponding energies ranging from 120 eV to 120 keV. At this energy regime there are a lot of ways of interaction between x-ray and atom, such as auger electrons, Compton scattering, elastic scattering and photoemission (Fig. 2.1). However, the most probable process is absorption of x-rays through photoelectric effect. In this process, an x-ray photon is absorbed by an electron in a tightly bound quantum core level (such as the 1s or 2p level) of an atom. The binding energy of this core level must be less than the energy of the incident x-ray. Otherwise, the bound electron will not be perturbed from this quantum state and will not absorb the x-ray. So if the binding energy of the electron is less than that of the x-ray, the electron may be probably removed from its quantum level. In this case, the x-ray is absorbed and any energy in excess of the electronic binding energy is given to a photo-electron which is ejected from the atom.

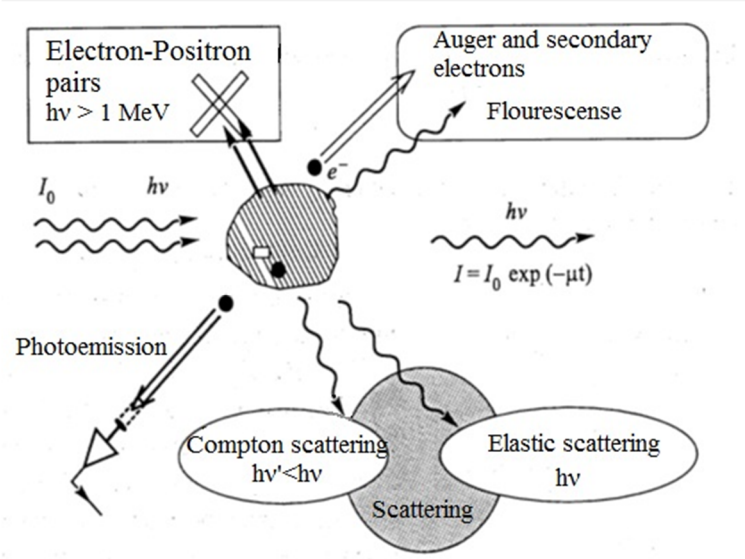

Figure 2.1 Interaction between X-ray and substance.

Process of x-ray absorption quantitate expressed through the absorption coefficient, μ which gives the probability that x-rays will be absorbed according to Beer's Law:

$$I = I_0 e^{-\mu d}, \qquad (2.1)$$

where I_0 is the x-ray intensity incident on a sample, d is the sample thickness, and I is the intensity after transmission through the sample.

When X-ray excites isolated atom, scattering cross section energy dependence is defined by selection rule $\Delta l=\pm 1$ and energy conservation $\delta(E_{final}-E_{initial}-\hbar\omega)$. So absorption coefficient behavior, which depends on cross section, is defined only by electron energy levels. If atom is not isolated, x-ray will excite photoelectron and it will scatter on potentials of surrounding atoms. So there will appear interference between this two electron waves and cross section (and absorption coefficient

as well) will get oscillating energy dependence XAFS (X-ray Absorption Fine Structure). Investigating of this oscillating function can give information about neighboring atoms (Fig. 2.2).

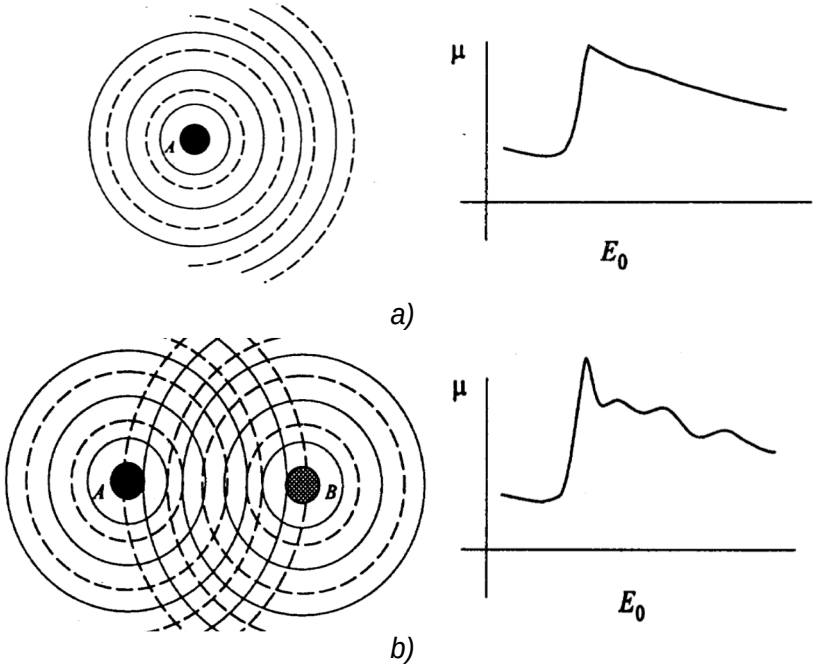

Figure 2.2 Exciting of a) isolated b) not isolated atom, and corresponding absorption coefficients.

XAFS is generally divided in two distinct ranges: the near-edge spectra XANES (X-ray Absorption Near Edge Structure) – typically within 30-50 eV of the main absorption edge, and the extended fine-structure EXAFS (Extended X-ray absorption fine structure) (Fig. 2.3). In first range photoelectron has low energy so dominant process is multiple scattering. For EXAFS dominant process is single scattering and this fact is used as main approximation for quantitate analysis of absorption spectra.

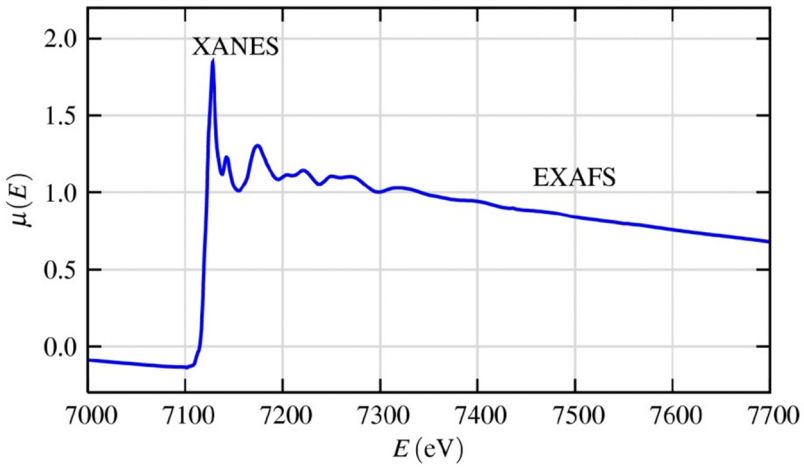

Figure 2.3 XAFS μ(E) for FeO. The measured XAFS spectrum is shown with the XANES and EXAFS regions identified [3].

This analysis starts from extracting EXAFS χ(k) function from absorption spectra, so its defined as

$$\chi(k) = \frac{\mu(k)-\mu_0(k)}{\mu_0(k)}, \quad (2.2)$$

where $\mu(k) = \frac{1}{d} ln(I/I_0)$ absorption coefficient; $\mu_0(k)$ - absorption coefficient of isolated atom, which defined as smooth decreasing function; *k* is wave vector of photoelectron, which is related with energy of incident X-ray.

So theoretical description of χ(k) function is given by EXAFS equation:

$$\chi(k) = \sum_j \frac{N_j S_0^2}{kR_j^2} f_j(k) e^{\frac{-2R_j}{\lambda(k)}} e^{-2k^2\sigma_j^2} sin\left(2kR_j + \vartheta_j(k)\right) \quad (2.3)$$

where $f_j(k)$ is scattering amplitude of neighboring atoms; N_j is number of neighbor atoms; R_j is radius of *j* coordination shell; *k* is a wave number of electron; $\lambda(k)$ is average free path of photoelectron in a solid; $\vartheta_j(k)$ is summary phase shift due to scattering neighbor atoms and excited atom; σ_j is coefficient that describes lattice distortion; S_0^2 appears because photon can give not all of its energy to photoelectron, but some of this energy can be used for ionization of another atomic shell (usually S_0^2 is ~0.7-1). Also, it should be noted that parameter σ_j is different from Debye Waller's factor, because it means lattice distortion relative to absorbing atom, not deviations from lattice sites. Factor $e^{\frac{-2R_j}{\lambda(k)}}$ describes process of photoelectron inelastic scattering on surrounding atoms. Contribution from long-distanced spheres is decreasing by factors $e^{\frac{-2R_j}{\lambda(k)}}$ and $\frac{1}{kR_j^2}$, also function $sin(2kR_j + \vartheta_j(k))$ becomes rapidly oscillating, which is not observable on experiment. So for getting result $\chi(k)$ we should sum only first 3-4 coordination spheres.

To get contribution from each sinusoid it's convenient to use Fourier transform for $\chi(k)$:

$$F(R) = \frac{1}{2\pi} \int_{-\infty}^{+\infty} \chi(k) e^{2ikR} dk \quad (2.4)$$

Maximums of *F(R)* corresponds to value *R*, which is radius of certain coordination spheres. Thus analysis of $\chi(k)$ gives information about neighbor atoms and their distribution on radius *R*.

2.2 Experimental setup

For measuring XAFS it is needed to have source of x-rays with tunable energy and quite high resolution ~1-1.5 eV. Also good detectors are required for uniform precise measurement of $\mu(E)$ before and after absorption edge – intensities in this ranges can reach difference up to 3 orders. Mistakes in measurements of $\mu(E)$ can degrade or even destroy this fine structure. So as x-ray source usually synchrotrons are used also in reason of high intensity of photon flux.

While charged particles (electrons or positrons) are turning in bending magnet of synchrotron they radiate x-rays with wide range of wavelengths. Monochromator, which consists of two similar crystals, uses Bragg's law for selecting photons with certain energy. After that radiation goes through exit slits to form required beam profile.

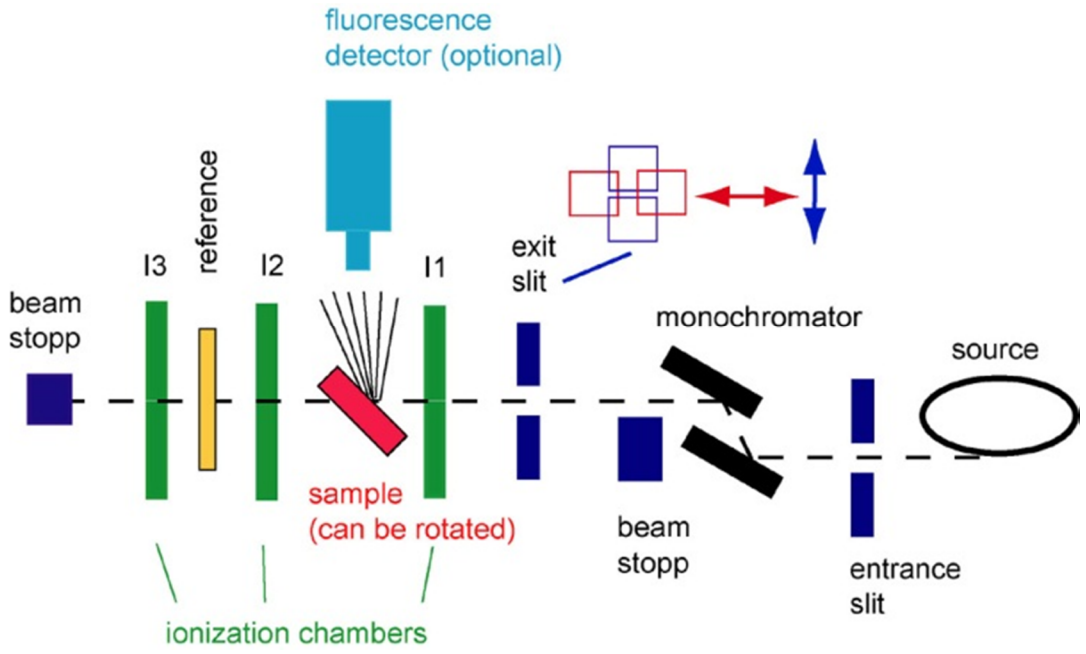

Figure 2.4 Experimental setup for measuring XAFS [4].

Beam with certain profile goes further through sample and ionization chambers. There are three ionization chambers, first two are used for obtaining $\mu(E)$: one measures current before sample, second measures current after transmission through the sample. Also there is reference, which is represented by metallic foil. Measurement of reference spectra is needed for energy calibration and reduction of monochromator's energy drift. Second and third ionization chambers are used for measuring $\mu(E)$ for this foil – that is needed for energy calibration. Sometimes beam can't go through the sample in reason of high absorption and in this case XAFS spectra are measured in fluorescence mode. To do it, sample is rotated and instead of ionization chambers 2 and 3, fluorescence detector is used.

So in experiment currents in ionization chambers and not intensities are measured. With reference data absorption coefficient for transmission mode transforms to $\mu=(1/d)[\ln(i_1/i_2)-\ln(i_2/i_3)]$, where i_1, i_2 and i_3 – currents in ionization chambers 1,2 and 3.

EXAFS spectra for Ti K-edge were got on A1 beamline at DORIS III, which monochromator can reach energy in range of 2.4-8.0 KeV.

3 Measurements

3.1 Sample holder

New sample holder was designed for investigation of phase transition in alloy $Ti_{0.5}Ni_{0.25}Cu_{0.25}$, which appears in temperature range of 30-70 ^{o}C. This holder consists of four parts: base, which attaches to cryostat, base plate, sample and Peltier modules. There are hole for temperature detector which is represented by thermocouple, and channel for cable for this detector, which are marked with arrow on figure 3.1. There is some feature that was planned for this design: sample should be placed on a diameter of round base for more convenient measurement of XAFS spectra in fluorescence case. That is important, because if sample is rotated and it's not on a certain position, then it could go out of beam. However it was impossible to design base plate position in certain place of base in reason of cryostat construction specifics, so sample is deviated for ~1 mm from base's diameter. This deviation is not a problem, because it is very small and beam hits sample even if it is rotated. There was a prototype of this sample holder, with which first spectra were measured (Fig. 3.2).

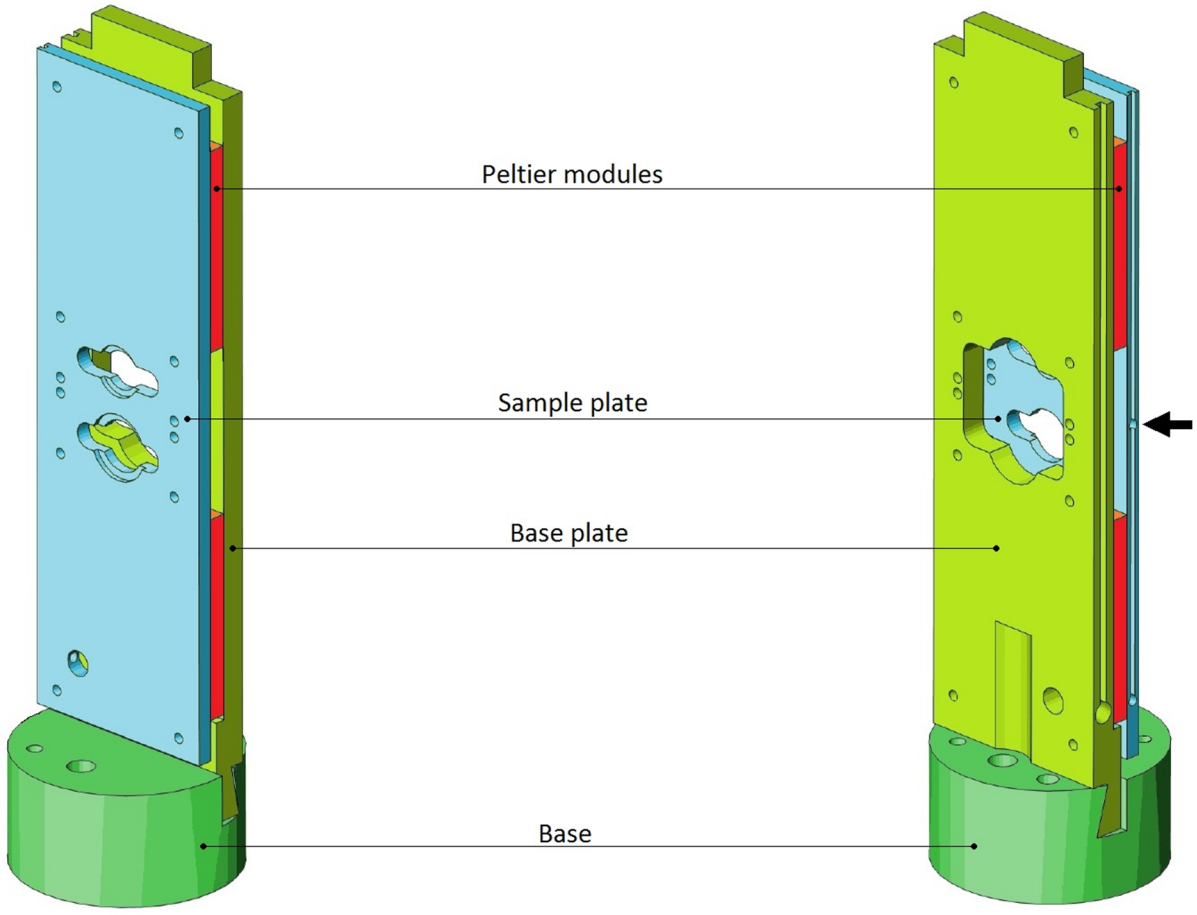

Figure 3.1 Design of new sample holder with temperature control.

Thermocouple and Peltier modules are connected to MTTC-1410 Thermoelectric controller to provide accurate temperature control and which is bi directional device, which could be used for heating and cooling the sample. During the measurements there were some problems with stability

of temperature – variation was about ±2 ^{o}C. Removing heat from cryostat by using cooled nitrogen gas helped to stabilization of temperature, however this problem didn't disappear completely.

3.2 Experiment and Data analysis

Spectra were measured in transmission mode on A1 beamline at DORIS III in temperature range of 30-70 ^{o}C. Sample was prepared for measuring by polishing the $Ti_{0.5}Ni_{0.25}Cu_{0.25}$ alloy foil. XAFS spectrum of Ti K-edge at room temperature is presented on figure 3.3.

Sample was not uniform, that's why at first measure attempts there were a lot of glitches and noise on spectra, which distorted fine structure. This problem appears when size of beam is big and its spatial position is not constant – if beam slightly moves than it hits sample in different position and this process produces glitches on spectra. After decreasing size of beam and finding the most uniform area on sample, that problem was almost solved.

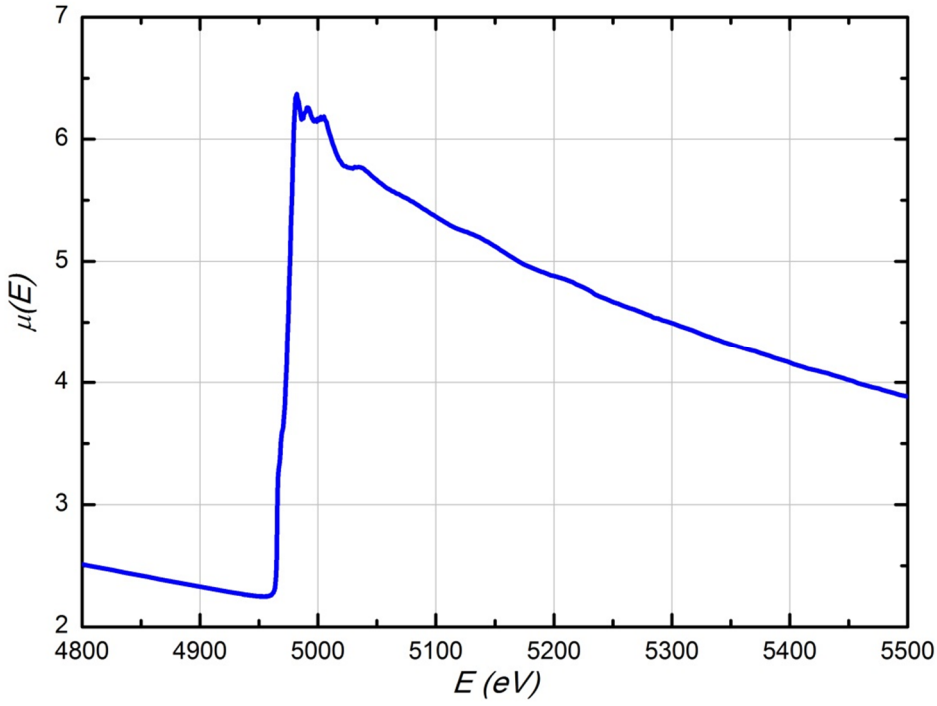

Figure 3.3 XAFS spectrum for $Ti_{0.5}Ni_{0.25}Cu_{0.25}$ at room temperature.

As it was mentioned above, there was a problem with stabilization of temperature during the measurements, so it was impossible to measure whole temperature range. Also, problem with noise and glitches was solved quite late and there is only one good spectrum at room temperature. So $Ti_{0.5}Ni_{0.25}Cu_{0.25}$ structure was investigated only in martensitic phase.

So after measuring XAFS spectra it is necessary to extract EXAFS $\chi(k)$ function as described in theory chapter (fig. 3.4). At this step $\chi(k)$ is multiplied to k^2 for increasing useful signal at the end of spectra. After that we use Fourier transform, but including additional multiplier to formula (2.4):

$$F(R) = \sqrt{\frac{2}{\pi}} \int_{k_{min}}^{k_{max}} k^n \chi(k) W(k) e^{-2ikr} dr \qquad (2.5)$$

This formula also contains window function *W(k)*, which is needed for decreasing noises in the end of spectrum and for decreasing XANES signal at the beginning of spectrum. EXAFS $\chi(k)$ function contains a lot of noise in the end, so this part is cut. As a consequence spatial resolution of Fourier transform is relatively low. Also it's obvious to see that FT$\{\chi(k)*k^2\}$ has only one peak, that's why this spectrum doesn't contain information about long range order (fig. 2.5).

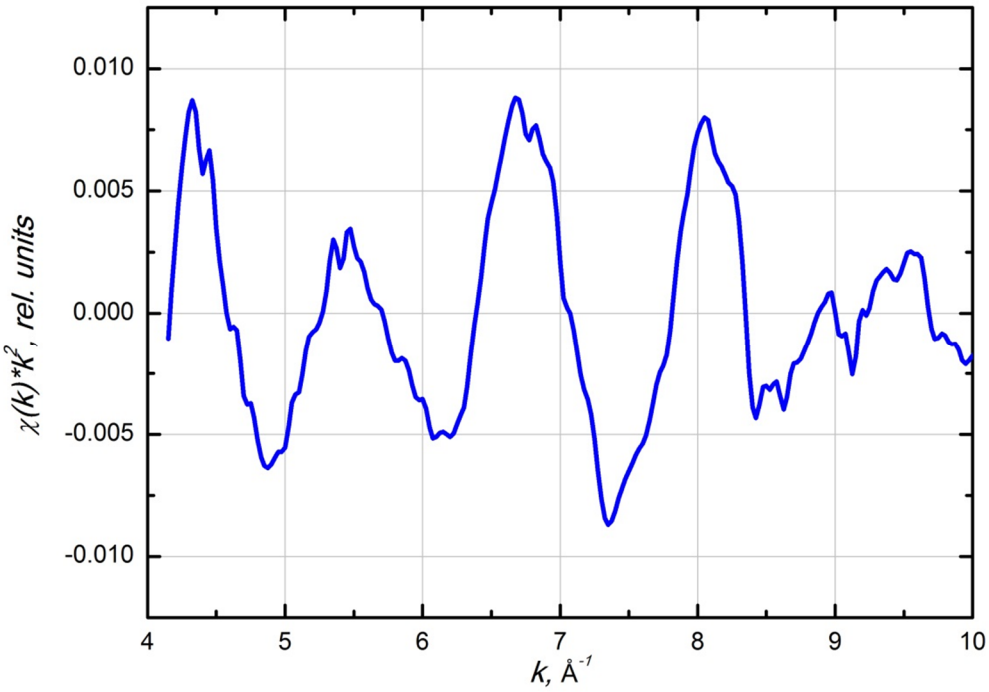

Figure 3.4 EXAFS $\chi(k)*k^2$ function for $Ti_{0.5}Ni_{0.25}Cu_{0.25}$ at room temperature.

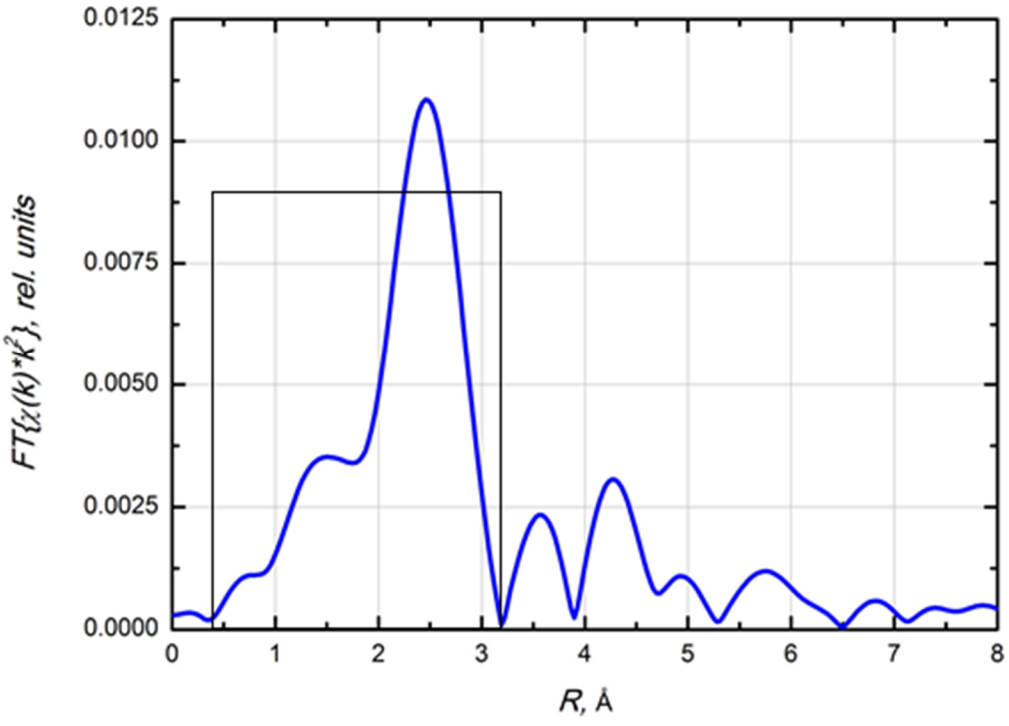

Figure 3.5 FT$\{\chi(k)*k^2\}$ function for $Ti_{0.5}Ni_{0.25}Cu_{0.25}$ at room temperature.

Now we put a window function and make back Fourier transform for EXAFS $\chi(k)$ function. After that structural data from introduction chapter is used for constructing a model spectrum with which information about local structure of Ti is got. So experimental $BFT[FT\{\chi(k)*k^2\}*W(R)]$ and model spectra are shown on figure 3.6. Also Fourier transforms of these functions are represented on figure 3.7.

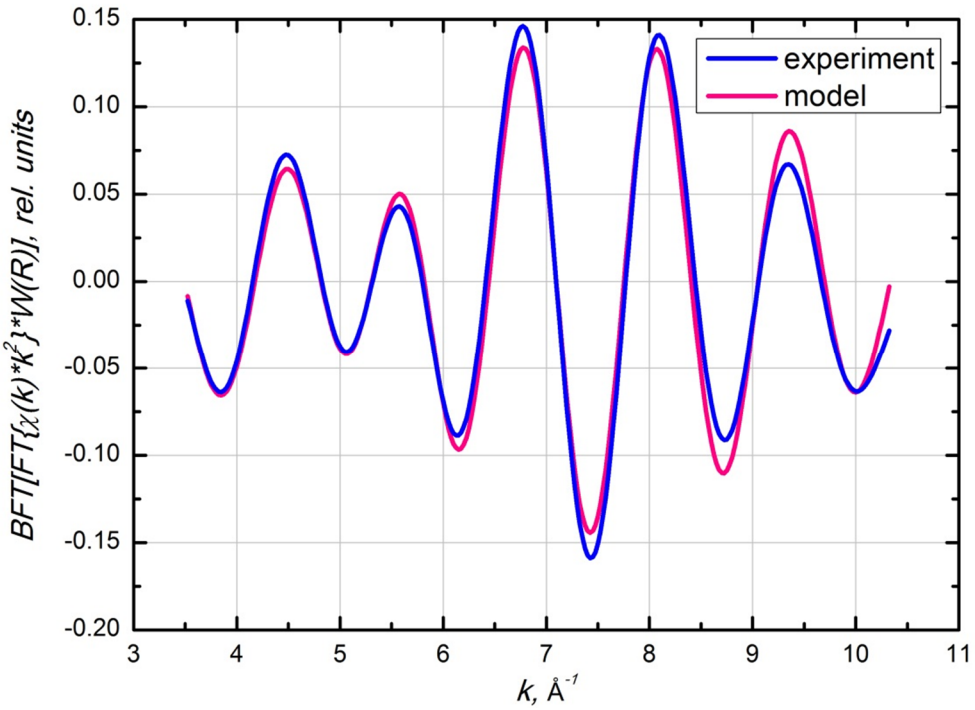

Figure 3.6 $BFT[FT\{\chi(k)*k^2\}*W(R)]$ function for $Ti_{0.5}Ni_{0.25}Cu_{0.25}$ at room temperature.

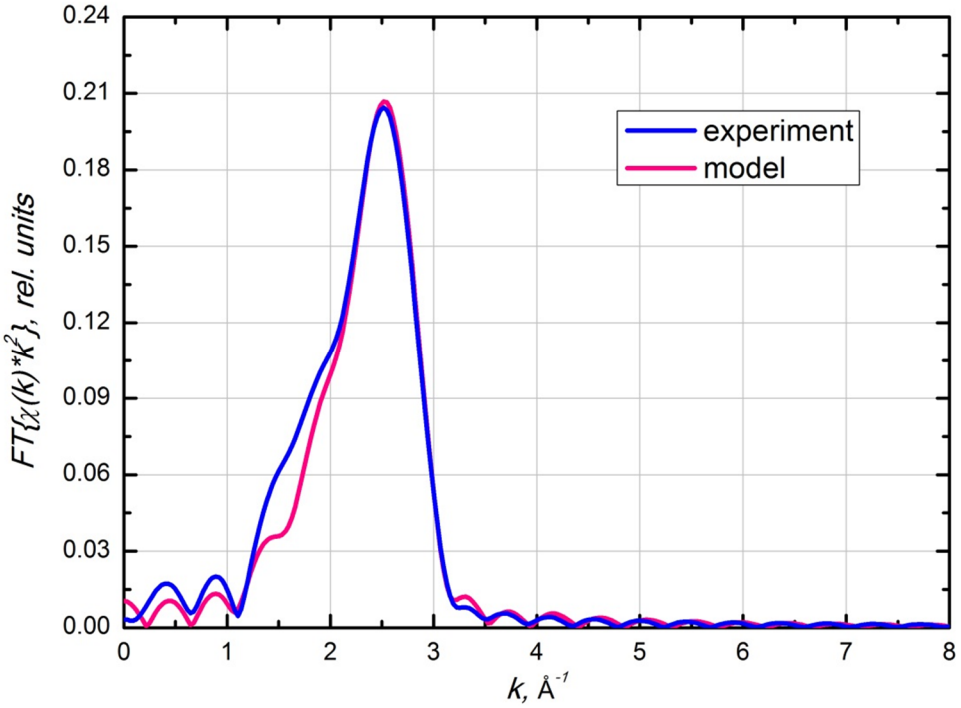

Figure 3.7 Fourier transforms of $BFT[FT\{\chi(k)*k^2\}*W(R)]$ and model $\chi(k)$ functions.

Before discussing fitting results, it is important to make next notes. First, input data for simulating model spectra does not contain information about different Cu and Ni crystallographic positions and in first approximation in this model Ni and Cu seem like they are in the same position in crystal. However in process of fitting coordination spheres with different sort of atoms are separating into different ones. As result we can distinguish spheres with Ti and Cu.

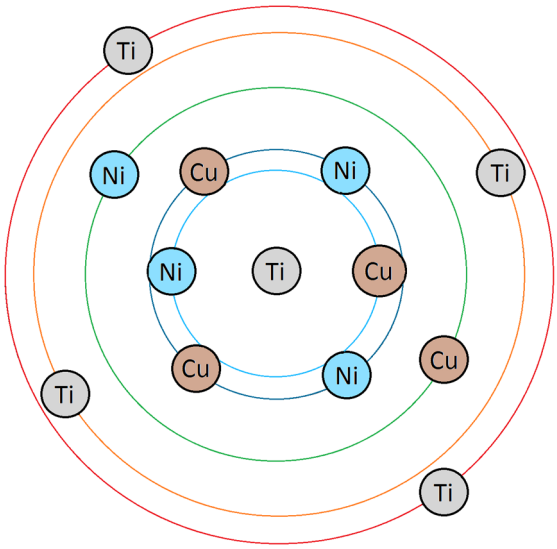

Figure 3.8 First coordination spheres for Ti in $Ti_{0.5}Ni_{0.25}Cu_{0.25}$ alloy are schematically shown. Spheres 1-2 and 4-5 have close radiuses.

Another point is about calculated radiuses for coordination shells. It is schematically shown on figure 3.8. Spheres 1 and 2 have almost equal radiuses which are $R_{1\ Ti\text{-}1Ni/Cu} = 2.58$ Å and $R_{2\ Ti\text{-}2Ni/Cu} = 2.61$ Å, so it is quite difficult to distinguish these shells. For spheres 4 and 5 there is the same situation: $R_{4\ Ti\text{-}2Ti} = 2.91$ Å and $R_{5\ Ti\text{-}2Ti} = 2.94$ Å. In that reason for successful data analysis it is necessary to put identical atoms to single spheres. It will decrease number of free parameters and increase precision of fitting.

As mentioned in introduction for calculating experimental data we used XAFS spectra for Ni and Cu K-edge. For this procedure three experimental absorption spectra were put as input data to VIPER software package. Fitting goes simultaneously on all edges by using three model spectra. In these models we fix number of neighbors and corresponding radiuses for identical distances (For example: Ti-2Ni distance for Ti spectrum equal to Ni-4Ti for Ni spectrum). So, by increasing number of spectra we increase number degrees of freedom for whole fitting, but also it is possible to fix some of parameters. As a consequence the same fitting for each spectra is done, but with less number of free parameters. By using of this feature fitting accuracy significantly increased.

The result from this fit gives next values for radiuses and disordering factors of first coordination shells:

$$R_{1\ Ti\text{-}Ni/Ti\text{-}2Ni} = 2.54\ Å, \qquad \sigma_1^2 = 0.040\ Å^2;$$
$$R_{2\ Ti\text{-}Ni} = 2.79\ Å, \qquad \sigma_2^2 = 0.011\ Å^2;$$
$$R_{3\ Ti\text{-}Cu/Ti\text{-}2Cu} = 2.63\ Å, \qquad \sigma_3^2 = 0.040\ Å^2;$$
$$R_{4\ Ti\text{-}Cu} = 2.82\ Å, \qquad \sigma_4^2 = 0.015\ Å^2;$$
$$R_{5\ Ti\text{-}2Ti/Ti\text{-}2Ti} = 3.05\ Å, \qquad \sigma_5^2 = 0.032\ Å^2;$$

Also as one of results of fitting it is necessary to introduce a quantitate parameter, which shows fitting accuracy. So R-factor is defined as

$$R = 100\left[\frac{\sum_{i=1}^{N_{pts}}\left(y_{i\,exp}-y_{i\,mod}\right)^2}{\sum_{i=1}^{N_{pts}}\left(y_{i\,exp}\right)^2}\right]^{1/2} \qquad (2.6)$$

where N_{pts} is number of points, $y_{i\ exp}$ and $y_{i\ mod}$ respectively denotes experimental and model $\chi(k)$ weighted by k^2. For $Ti_{0.5}Ni_{0.25}Cu_{0.25}$ fitting seems not very successful because R-factor in this case is 18.65 %.

It is remarkable, that disordering factors for coordination shells, which combine pairs of calculated shells, are bigger then distortion factors for single spheres. Combination of spheres with slightly different radiuses gives significant distortion and also it causes effect on fitting accuracy, that's why R-factor is high.

4 Summary

1. New sample holder, which provides cooling and heating the sample in temperature range of 20-100 ^{o}C, was designed.
2. XAFS spectrum for Ti K-edge was measured for shape memory alloy $Ti_{0.5}Ni_{0.25}Cu_{0.25}$ at room temperature on beamline A1 at DORIS III.
3. Ti local structure in $Ti_{0.5}Ni_{0.25}Cu_{0.25}$ in martensitic phase was investigated by means of EXAFS-spectroscopy.
4. Simultaneous fitting on K-edges of Ti, Cu and Ni highly increased precision of results.

5 References

[1] Alexander Yaroslavtsev, Alexey Menushenkov, Roman Chernikov, Olga Grishina, Yan Zubavichus, Alexey Veligzhanin, Alexander Shelyakov and Nikolay Sitnikov: Local structure of TiNiCu(Hf) shape memory alloys: XAFS data analysis; Z. Kristallogr. 225 (2010) 478–481 / DOI 10.1524/zkri.2010.1303 Z. Kristallogr. 225 (2010) 478–481 / DOI 10.1524/zkri.2010.1303

[2] P.L. Potapov, S. E. Kulkova, A. V. Shelyakov, K. Okutsu, S. Miyazaki, D Schryvers: Crystal structure of orthorhombic martensite in TiNi-Cu and Ti-Ni-Pd intermetallics; J. Phys. IV France 112 (2003)

[3] Matthew Newville: Fundamentals of XAFS, Revision 1.6 July 22, 2004

[4] http://hasylab.desy.de/facilities/doris_iii/beamlines/c_cemo/index_eng.html

[5] K. V. Klementev, VIPER for Windows (Visual Processing in EXAFS Researches), freeware, http://www.crosswinds.net/~klmn/viper.html

[6] K V Klementev, Extraction of the fine structure from x-ray spectra, *J. Phys. D: Appl. Phys., 34, 2001, pp. 209-217*

[7] Otsuka k. and Ren X., Intermetallics 7(1999) 511-528

[8] Official SALOME site http://www.salome-platform.org/

[9] Offcial 3D-Tool site http://www.3d-tool.de/english/cad-viewer.htm

[10] Offcial FEFF site http://leonardo.phys.washington.edu/feff/